Table 1. The *XMM–Newton* RGS1 observations of RX J0720.4−3125 in chronological order. We list the exposure times and the net counts after the data passed the GTI filters.

Obs. ID	Date	Counts 0.35–1.0 keV	Eff. exposure (ks)
0124100101	2000 May 13	11 480	42.36
0132520301	2000 Nov 21	7878	30.24
0156960201	2002 Nov 6	7518	29.61
0156960401	2002 Nov 8	7796	31.22
0158360201	2003 May 2	15 507	61.56
0161960201	2003 Oct 27	13 513	44.67
0164560501	2004 May 22	8007	26.97
0300520201	2005 Apr 28	10 366	37.97
0300520301	2005 Sep 22	10 034	36.33
0311590101	2005 Nov 12	10 917	39.57
0400140301	2006 May 22	5952	21.62
0400140401	2006 Nov 5	5592	21.82
0502710201	2007 May 5	4451	16.77
0502710301	2007 Nov 17	6138	24.81
0554510101	2009 Mar 21	3682	15.45
0601170301	2009 Sep 22	3570	15.61
0650920101	2011 Apr 11	4443	19.81
0670700201	2011 May 02	3741	16.99
Total		140 584	533.38

Therefore, we fitted the co-added RGS1 spectrum keeping all parameters free for fitting but fixed the line energy of the cyclotron line at 0.3 keV (also for the error calculations).

We fitted the RGS1 spectrum with this model, using the photons from 0.35 to 1.0 keV. The co-added spectrum fits with χ^2/degrees of freedom (d.o.f.) = 1.50. For the narrow absorption feature, we included a further Gaussian line at 0.57 keV. The fit including the narrow absorption feature yields χ^2/d.o.f. = 1.42. Note that no instrumental features are present around 0.57 keV, i.e. supporting an astrophysical origin. The fit results are listed in Table 8 and the spectrum is shown in Fig. 1.

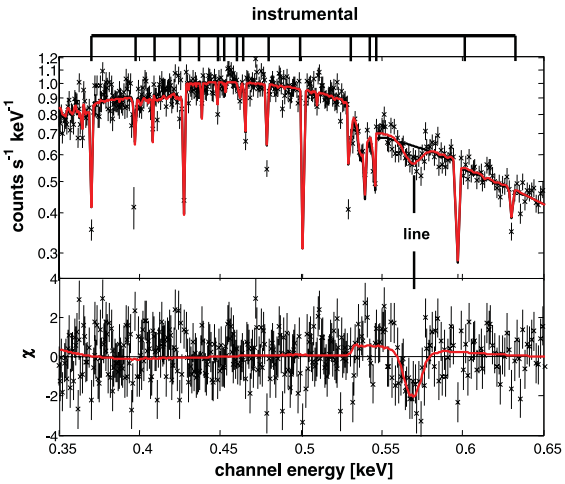

Figure 1. The co-added RGS1 (first-order) spectrum of RX J0720.4−3125 with a total exposure of 533 ks. The thin, solid black line represents the fit model, while the lower red line shows the fit model plus a narrow absorption feature seen at $568.6^{+1.8}_{-1.9}$ eV with EW = $-1.89^{+0.56}_{-0.62}$ eV (errors denote 90 per cent confidence level), see also Hambaryan et al. (2009) for comparison. We also mark the locations of instrumental features exemplarily in this figure (not shown in the spectra of the other NSs).

We confirm the presence of a narrow absorption feature at $568.6^{+1.8}_{-1.9}$ eV with an equivalent width (EW) of EW = $-1.89^{+0.56}_{-0.62}$ eV (that corresponds to 5.6σ significance).

2.2 RX J1308.6+2127 (RBS1223)

The *XMM–Newton* EPIC-pn spectra of the M7 member RX J1308.6+2127 exhibit two broad Gaussian absorption features (Haberl 2007) with line energies of 0.30 and 0.23 keV (or one line at 0.30 or 0.29 keV; see Haberl et al. 2003), again below the RGS spectrum. Thus, these two lines appear as one broader line with a line energy at 0.205 keV, i.e. we use the XSPEC model phabs*(bbodyrad+gaussian) and fixed the line energy for fitting, but released it for the error calculation. The *XMM–Newton* RGS observations of RX J1308.6+2127 sum up to 190 ks, where 170 ks are left after passing the GTI filters; see Table 2.

The co-added spectrum fits with χ^2/d.o.f. = 1.32. Although having less counts than the co-added spectrum of RX J0720.4−3125, it can be clearly stated that no significant narrow absorption feature at 0.57 keV is detected. However, the model overpredicts the count numbers in the energy range from 0.48 to 0.60 keV, which can be interpreted as a new absorption feature – broader than the absorption feature in RX J0720.4−3125, but too narrow to be detected in EPIC-pn.

Including a further (broader) Gaussian absorption line at 0.53 keV decreases χ^2/d.o.f to 1.13. The co-added RGS1 spectrum is shown in Fig. 2. Schwope et al. (2007) reported one absorption feature at 0.20–0.39 keV and a further broad feature at either 0.46 or 0.73 keV in the *XMM–Newton* EPIC-pn spectra of RX J1308.6+2127. The second feature does not correspond to the line at 0.53 keV found here and there is no evidence for the feature found in Schwope et al. (2007) in our co-added RGS1 spectrum. The differences between RGS and pn were reduced in the last years [e.g. compared to Haberl et al. (2003) and Schwope et al. (2007)] due to new calibrations. Thus, an updated combined RGS and pn analysis is required with the new calibrations.

Maybe the X-ray spectrum of RX J1308.6+2127 is much more complex and the absorption features change with time [since the work of Schwope et al. (2007), we have five more observations available]. We stress that the RGS detector exhibits strong features in the energy range from 0.48 to 0.60 keV, but these features are narrow compared to the feature we found at 0.53 keV (that is not seen in the brighter spectrum of e.g. RX J0720.4−3125).

Table 2. As in Table 1, but for RX J1308.6+2127 (RBS1223).

Obs. ID	Date	Counts 0.35–1.0 keV	Eff. exposure (ks)
0090010101	2001 Dec 31	946	8.83
0157360101	2003 Jan 1	3055	28.71
0163560101	2003 Dec 30	3019	29.80
0305900201	2005 Jun 25	1633	16.73
0305900301	2005 Jun 27	1487	14.74
0305900401	2005 Jul 15	1230	12.43
0305900601	2006 Jan 10	1576	16.72
0402850301	2006 Jun 8	545	5.53
0402850401	2006 Jun 16	842	8.34
0402850501	2006 Jun 27	913	9.48
0402850901	2006 Jul 5	662	7.11
0402850701	2006 Dec 27	993	10.34
Total		16 901	168.76

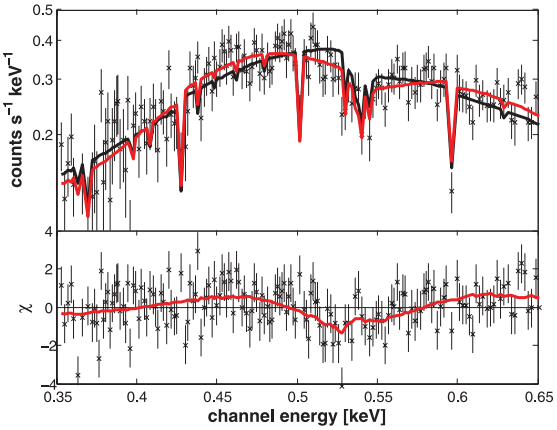

Figure 2. As in Fig. 1, but for RX J1308.6+2127 with a total exposure of 170 ks. The new absorption feature is seen at $535.3^{+7.4}_{-13.4}$ eV with EW $= -20^{+10}_{-13}$ eV (errors denote 90 per cent confidence level). There is no absorption feature at 0.57 keV

Thus, the new absorption feature is not of an instrumental origin.

Since the line centre of the new absorption feature lies at 0.53 keV [the absorption energy of O I at rest; see also de Vries et al. (2003)], we used the XSPEC absorption model vphabs to vary the abundance of oxygen during the fit procedure. The fit did not find a solution to compensate the absorption feature at 0.53 keV with a higher abundance of neutral oxygen, hence this feature may originates from the NS itself.

The fit results are listed in Table 8.

2.3 RX J1605.3+3249

The first report of a narrow absorption feature in the co-added RGS spectra of an isolated NS was published by van Kerkwijk et al. (2004), who found an absorption line at 0.57 keV in the spectra of RX J1605.3+3249. Since then, nine further *XMM–Newton* observations of RX J1605.3+3249 were performed, i.e. 14 in total. However, almost all observations after 2006 February are strongly contaminated by high background and did not pass the GTI filtering. Finally, our sample of observations is not much different from that used by van Kerkwijk et al. (2004); see Table 3. We only could add observation 0302140501 (6 ks left after GTI filtering), but omitted observation 0302140601 (used in van Kerkwijk et al. 2004). The total exposure time sums up to 110 ks.

van Kerkwijk et al. (2004) found a broad absorption feature at 0.493 keV, again associated with a possible cyclotron line, i.e. we use the model phabs*(bbodyrad+gaussian) here too. This line energy lies well within the RGS energy range, but the best fit leads to a line energy at 0.403 keV that has to be fixed for the error calculation. Therefore, the $N_{\rm H}$ value and the blackbody temperature lie below the values listed in van Kerkwijk et al. (2004), but are consistent within the errors; see Table 8. The co-added spectrum fits with χ^2/d.o.f. = 1.22.

Table 3. As in Table 1, but for RX J1605.3+3249.

Obs. ID	Date	Counts 0.35–1.0 keV	Eff. exposure (ks)
0073140301	2002 Jan 9	2717	20.08
0073140201	2002 Jan 15	3715	27.83
0073140501	2002 Jan 19	3009	22.21
0157360401	2003 Jan 17	4470	30.98
0302140501	2006 Feb 12	748	5.91
Total		14 660	107.01

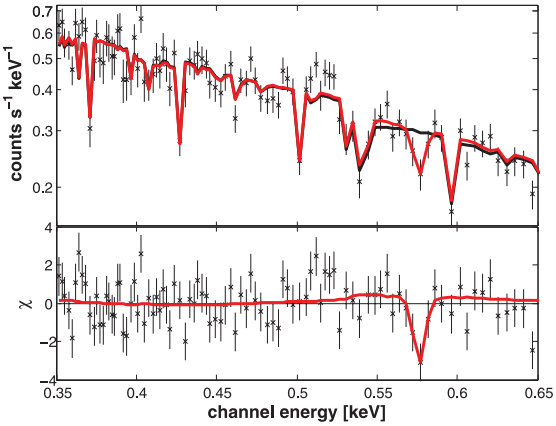

Figure 3. As in Fig. 1, but for RX J1605.3+3249 with a total exposure of 110 ks. The narrow absorption feature is seen at $576.1^{+2.5}_{-2.7}$ eV with EW $= -3.2^{+1.5}_{-1.8}$ eV (errors denote 90 per cent confidence level); see also van Kerkwijk et al. (2004), for comparison.

Adding a further Gaussian absorption feature, the fit yields χ^2/d.o.f. = 1.11. We confirm the presence of an absorption line at $576.1^{+2.5}_{-2.7}$ eV with EW $= -3.2^{+1.5}_{-1.8}$ eV, with the 3.5σ significance, as reported in van Kerkwijk et al. (2004). The co-added RGS spectrum of RX J1605.3+3249 is shown in Fig. 3.

2.4 RX J1856.4−3754

This NS is the brightest member of the M7, is known to exhibit no features in *XMM–Newton* EPIC-pn and *Chandra* High Resolution Camera (HRC)-S/Low Energy Transmission Grating (LETG) spectra (Burwitz et al. 2001, 2003), and is constant over time. Thus, RX J1856.4−3754 is used as calibration source for X-ray telescopes. Therefore, the *XMM–Newton* observations sum up to 1000 ks, where 880 ks remain after the GTI filtering; see Table 4. Although Burwitz et al. (2001, 2003) found no absorption feature we include this source as well, since the co-added RGS spectra of RX J1856.4−3754 were not investigated before.

Likewise Burwitz et al. (2001, 2003), we apply the XSPEC model phabs*(bbodyrad), where the fit yields χ^2/d.o.f. = 1.16 (see Table 8). The spectrum of RX J1856.4−3754 is completely featureless in the RGS1 energy range (Fig. 4).

2.5 Geminga (PSR J0633+1746)

The first spectrum of Geminga with a sufficiently large count number was published by Halpern & Ruderman (1993), using *ROSAT* data. They found the Geminga spectrum is best modelled with two blackbodies having $kT_{\rm eff} = 43$ and 260 eV, respectively. Using new *ROSAT* data, Halpern & Wang (1997) identified a power-law component above 2 keV with $\Gamma = 0.5$–1.5 (the most recent value is $\Gamma = 1.72 \pm 0.10$; see Jackson et al. 2002; Caraveo et al. 2004). Therefore, we use phabs*(bbodyrad+bbodyrad+pow) for the data fitting.

Although Geminga was frequently observed with *XMM–Newton* (240 ks after GTI filtering), the total number of counts is only 3100, i.e. less than half the photons (Halpern & Ruderman 1993) could use

Table 4. As in Table 1, but for RX J1856.4−3754.

Obs. ID	Date	Counts 0.35–1.0 keV	Eff. exposure (ks)
0106260101	2002 Apr 8	8417	57.30
0201590101	2004 Apr 17	5158	36.61
0165971701	2004 Sep 24	4742	33.73
0165971601	2004 Sep 24	4654	33.29
0165971901	2005 Mar 23	2531	17.91
0213080101	2005 Apr 15	1579	11.39
0165972001	2005 Sep 24	4624	33.53
0165972101	2006 Mar 26	8953	68.71
0412600101	2006 Oct 24	8715	72.75
0412600201	2007 Mar 14	6049	50.24
0415180101	2007 Mar 25	3042	22.72
0412600301 (S004)	2007 Oct 4	2926	22.25
0412600301 (U002)	2007 Oct 4	2459	19.69
0412600401	2008 Mar 13	6052	48.34
0412600601	2008 Oct 4	7913	64.97
0412600701	2009 Mar 19	8300	68.65
0412600801 (S004)	2009 Oct 7	872	6.90
0412600801 (U002)	2009 Oct 7	8576	70.88
0412600901	2010 Mar 22	8652	72.22
0412601101	2010 Sep 28	7950	68.30
Total		112 170	880.38

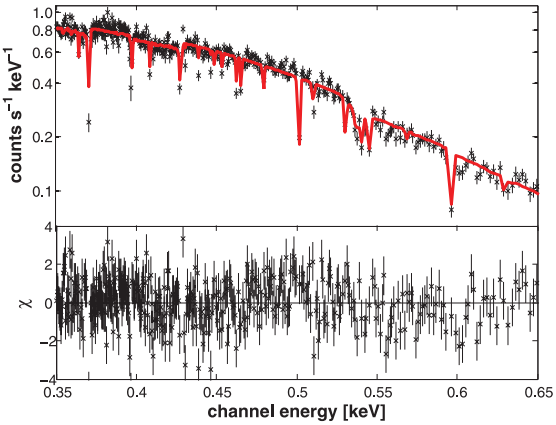

Figure 4. As in Fig. 1, but for RX J1856.4−3754 with a total exposure of 880 ks. The spectrum of RX J1856.4−3754 exhibits no spectral lines.

in their first Geminga spectrum (but with lower spectral resolution); see Table 5.

Since the co-added RGS spectrum of Geminga has the lowest count number in our sample and the hot blackbody dominates the spectrum above 1 keV, but is strongly superimposed by the power law (see e.g. fig. 1 in De Luca et al. 2005). We find the best fit with a negligible normalization of the hot blackbody, whereas the power law is clearly visible. Thus, we applied the model phabs*(bbodyrad+pow). The fit yields χ^2/d.o.f. = 1.21 and the results are shown in Table 8.

We find no evidence for an absorption feature like in the case of RX J0720.4−3125, RX J1308.6+2127 or RX J1605.3+3249 in the co-added RGS spectrum of Geminga. However, weak features cannot be detected due to the low count number (Fig. 5).

Table 5. As in Table 1, but for Geminga.

Obs. ID	Date	Counts 0.35–2.0 keV	Eff. exposure (ks)
0111170101	2002 Apr 4	993	76.38
0201350101	2004 Mar 13	259	15.85
0301230101	2005 Sep 16	49	4.91
0311591001	2006 Mar 17	521	34.80
0400260201	2007 Oct 2	228	20.17
0400260301	2007 Mar 11	277	21.71
0501270201	2007 Sep 18	211	22.73
0501270301	2008 Mar 8	127	11.82
0550410201	2008 Oct 3	240	21.11
0550410301	2009 Mar 10	181	11.36
Total		3086	240.84

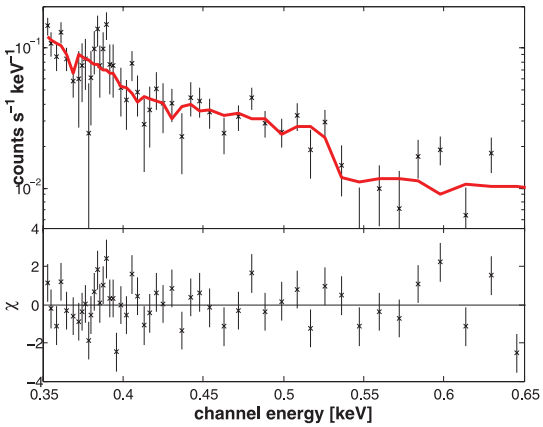

Figure 5. As in Fig. 1, but for Geminga (with a total exposure of 240 ks) fitted with one single blackbody and an additive power-law component. The spectrum of Geminga exhibits no lines.

2.6 PSR B0656+14

The first investigation of the emission of PSR B0656+14 was performed with *ROSAT* data by Possenti, Mereghetti & Colpi (1996), who modelled the spectrum with a blackbody and a second component that could be either a further blackbody or a power law. Later, Greiveldinger et al. (1996) applied the three-component model (two blackbodies and a power law with $\Gamma = 1.5 \pm 1.1$) that yields the best fit. This model was later confirmed by Pavlov, Zavlin & Sanwal (2002) using *Chandra* data. Marshall & Schulz (2002) found no evidence for spectral features in the *Chandra* spectra of PSR B0656+14, but used only two blackbodies (and no power law) for their fit model. Today, only one RGS observation of PSR B0656+14 is available (Table 6). But this observation yields more counts than e.g. all Geminga observations in total.

We first fitted the RGS1 spectrum of PSR B0656+14 with phabs*(bbodyrad+bbodyrad+pow). Both blackbodies dominate the spectrum in the RGS energy range, but the power law becomes significant above 2 keV (see fig. 2 in De Luca et al. 2005), where the RGS1 spectrum has much less counts. Thus, the power law is

Table 6. As in Table 1, but for PSR B0656+14.

Obs. ID	Date	Counts 0.35–2.0 keV	Eff. exposure (ks)
0112200101	2001 Oct 23	7483	38.12

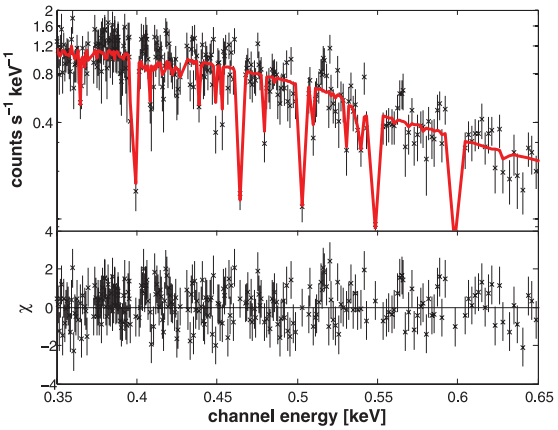

Figure 6. As in Fig. 1, but for PSR B0656+14 with a total exposure of 38 ks. The spectrum of PSR B0656+14 exhibits no lines.

negligible and we further on use the model phabs*(bbodyrad+bbodyrad) (likewise in Marshall & Schulz 2002). The fit yields χ^2/d.o.f. = 0.88 and the spectral properties are listed in Table 8.

We find no evidence for a narrow absorption feature in the RGS1 spectrum of PSR B0656+14 (Fig. 6) and thereby confirm the results in Marshall & Schulz (2002). The count number of the RGS1 spectrum would have been sufficiently high to detect an absorption feature as found e.g. in the spectrum of RX J0720.4−3125, if present.

2.7 PSR B1055−52

The first spectral investigation of PSR B1055−52 was performed by Oegelman & Finley (1993) using *ROSAT* data. Like in the case of PSR B0656+14, the best-fitting model required a blackbody and a further component that could be a second blackbody or a power law with $\Gamma \approx 4$. Combining *ROSAT* and *Chandra* data, Pavlov et al. (2002) showed that an adequate fit model requires three components: two blackbodies and a power law with $\Gamma \approx 1.7$. Therefore, we first use phabs*(bbodyrad+bbodyrad+pow).

Altogether, the RGS1 data of PSR B1055−52 sum up to 95 ks (90 ks after GTI filtering) with ≈4000 photons (Table 7). For the same reasons as discussed in the case of Geminga, we found the best fit for a negligible normalization of the second, hotter blackbody. Therefore, we applied the model phabs*(bbodyrad+pow) that fits with χ^2/d.o.f. = 1.16 (Table 8).

In contrast to the other 3M, PSR B1055−52 seems to exhibit a weak absorption feature at 0.57 keV, similar to those found in the co-added RGS1 spectra of RX J0720.4−3125 and RX J1605.3+3249. To check this, we add a Gaussian absorption line to our fit model (Fig. 7). With the new model, the χ^2/d.o.f. value does not change significantly to χ^2/d.o.f. = 1.15, but the fit easily finds its minimum with the new line at $565.0^{+26.0}_{-7.3}$ eV with EW = $-5.7^{+4.6}_{-9.2}$ eV. This feature is not consistent to the continuum within 2σ, i.e. less significant than the narrow absorption feature in RX J1605.3+3249, but we stress that the total count number in the case of the co-added RGS1 spectrum of PSR B1055−52 is more than three times less than in the case of RX J1605.3+3249, i.e. further observations are required to verify this absorption feature.

Table 7. As in Table 1, but for PSR B1055−52.

Obs. ID	Date	Counts 0.35–2.0 keV	Eff. exposure (ks)
0113050101	2000 Dec 14	1109	22.75
0113050201	2000 Dec 15	2323	55.66
0113050801	2000 Dec 15	164	3.77
0113050901	2000 Dec 15	356	7.84
Total		3952	90.02

2.8 *XMM–Newton* results

We co-added all available RGS data of the four brightest M7 (RX J0720.4−3125, RX J1308.6+2127/RBS1223, RX J1605.3+3249 and RX J1856.4−3754) and the 3M (Geminga, PSR B0656+14 and PSR B1055−52). We confirm the narrow absorption features at 0.57 keV in the spectra of RX J0720.4−3125 and RX J1605.3+3249 as reported in earlier work by Hambaryan et al. (2009) and van Kerkwijk et al. (2004), respectively. We found a new absorption feature at 0.53 keV in the co-added RGS spectrum of RX J1308.6+2127 that is broader than those found in the case of RX J0720.4−3125 and RX J1605.3+3249.

The co-added spectra of RX J1856.4−3754 and PSR B0656+14 are featureless, while the count number in the co-added spectra of Geminga is not sufficiently high to exclude such weak features. There might be a new absorption feature (comparable to those in the spectra of RX J0720.4−3125 and RX J1605.3+3249) present in the co-added spectrum of PSR B1055−52.

We fitted the absorption features using an additive Gaussian line and checked our results with the multiplicative gabs model. For both models we obtain exact the same values for the EWs.[4]

Our results are summarized in Table 8 and we will discuss them in the next sections.

3 THE *Chandra* HRC-S/LETG SPECTRA OF RX J0720.4−3125 AND RX J1856.4−3754

Hambaryan et al. (2009) considered the absorption feature at 0.57 keV could be caused by gravitational redshifted O VIII. If true, O VII should appear at 0.48 keV with the same redshift ($g_r = 1.17$, see the more detailed discussion in Section 4). However, we found no evidence for such a feature in the co-added RGS spectrum (see Fig. 1). Therefore, we also analysed the *Chandra* HRC-S/LETG spectra of RX J0720.4−3125[5] and RX J1856.4−3754 for comparison, since RX J1856.4−3754 does not exhibit any features in the *Chandra* HRC-S/LETG spectra (Burwitz et al. 2001, 2003).

The *Chandra* HRC-S/LETG (Juda 1996, 1997; Evans 1997; Kraft et al. 1997) data were analysed with CIAO 4.1. We created our own GTI files using DMGTI and filtered those events for data reduction with less than 60–180 count s^{-1} (depending on observation and background light curves). The photons (source plus background

[4] The documentation of gabs in the XSPEC manual is misleading and might cause some confusion. The τ (parameter 3) in gabs is not the optical depth (although it is even called so in older manuals). The 'correct' optical depth can be calculated by $\tau = \tau_{\rm xspec}/P_2/\sqrt{2\pi}$, where P_2 is the second parameter in the gabs model. This should be taken into account if EWs have to be calculated. We thank Oleg Kargaltsev, who pointed this out (see also http://xspector.blogspot.com/2011/07/note-on-gabs-model.html).

[5] RX J1605.3+3249 and RX J1308.6+2127 (RBS1223) are not as frequently observed as RX J0720.4−3125 with *Chandra* HRC-S/LETG. For example the 900-ks HRC-S/LETG observation of RX J1308.6+2127 has four times less counts than the co-added RGS spectrum. Thus, we do not discuss these spectra in this work.

Table 8. Fit results from the co-added *XMM–Newton* RGS spectra of four M7 and the 3M. The sizes of the emitting areas (norm) are calculated from the normalizations of the X-ray blackbodies and correspond to a distance of 300 pc, except in the case of RX J1856.4−3754 (130 pc; Walter et al. 2010) and PSR B1055−52 (750 pc; Kramer et al. 2003). The line energies of the broad absorption features are always fitted as free parameters (except in the case of RX J0720.4−3125, where the line energy was always fixed), but fixed for the error calculation. The EWs of these broad absorption features have no errors since the lines reach partly out of the energy range of the RGS spectrum. All errors denote 90 per cent confidence level.

Model component	Unit	RX J0720.4−3125	RX J1308.6+2127	RX J1605.3+3249	RX J1856.4−3754	Geminga	PSR B0656+14	PSR B1055−52
$N_{\rm H}$	$10^{20}\,{\rm cm}^{-2}$	$1.60^{+0.52}_{-0.65}$	$1.6^{+1.6}_{-1.5}$	$0.72^{+1.72}_{-0.72}$	≤ 0.32	$3.9^{+11.1}_{-1.9}$	$0.12^{+1.64}_{-0.12}$	$2.4^{+3.4}_{-2.4}$
bbodyrad$_1$								
kT_1	eV	$85.0^{+1.7}_{-1.6}$	$78.3^{+3.6}_{-3.3}$	$85.3^{+3.1}_{-4.2}$	$62.67^{+0.25}_{-0.60}$	$33.2^{+9.2}_{-12.1}$	$67.9^{+3.6}_{-6.7}$	$72.0^{+9.5}_{-7.8}$
norm$_1$	km	$6.47^{+0.64}_{-0.61}$	$6.7^{+1.8}_{-1.4}$	$4.81^{+1.44}_{-0.72}$	$5.015^{+0.260}_{-0.035}$	≤ 68	$9.53^{+4.66}_{-0.72}$	$8.8^{+4.3}_{-4.0}$
bbodyrad$_2$		–	–	–	–	–		–
kT_2	eV	–	–	–	–	–	170^{+36}_{-44}	–
norm$_2$	km	–	–	–	–	–	$0.373^{+0.608}_{-0.088}$	–
Gaussian$_1$					–	–	–	–
lineE$_1$	eV	300 (fixed)	205.83 (fixed)	403 (fixed)	–	–	–	–
σ_1 width	eV	$100.7^{+8.5}_{-12.4}$	$135.7^{+2.5}_{-3.2}$	$100.1^{+7.0}_{-5.7}$	–	–	–	–
EW$_1$	eV	−35.2	−163	−65.2	–	–	–	–
Power law		–	–	–	–		–	
Γ		–	–	–	–	$2.67^{+1.75}_{-0.91}$	–	$3.8^{+1.8}_{-2.4}$
norm	ph keV^{-1} cm^{-2} s^{-1} @1 keV	–	–	–	–	$9.1^{+4.5}_{-2.3}\times 10^{-5}$	–	$7.6^{+4.0}_{-4.3}\times 10^{-5}$
$\chi^2_{\rm red}$/d.o.f.		1.50/456	1.32/208	1.22/110	1.16/759	1.21/66	0.88/305	1.16/121
Gaussian$_2$					–	–	–	
lineE$_2$	eV	$568.6^{+1.8}_{-1.9}$	$535.3^{+7.4}_{-13.4}$	$576.1^{+2.5}_{-2.7}$	–	–	–	$565.0^{+26.0}_{-7.3}$
σ_2 width	eV	$4.8^{+1.8}_{-1.9}$	35^{+21}_{-18}	$3.3^{+4.1}_{-3.3}$	–	–	–	$5.6^{+20.1}_{-5.6}$
EW$_2$	eV	$-1.89^{+0.56}_{-0.62}$	-20^{+10}_{-13}	$-3.2^{+1.5}_{-1.8}$	–	–	–	$-5.7^{+4.6}_{-9.2}$
Significance	σ	5.6	3.2	3.5	–	–	–	2.1
$\chi^2_{\rm red}$/d.o.f.		1.42/453	1.13/205	1.11/107	–	–	–	1.15/118

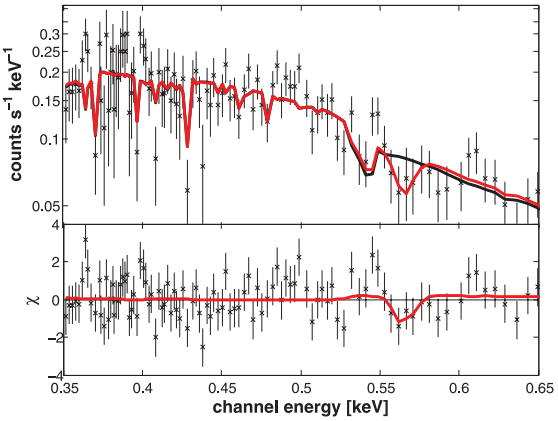

Figure 7. As in Fig. 1, but for PSR B1055−52 with a total exposure of 90 ks. The spectrum of PSR B1055−52 exhibits a new absorption feature seen at $565.0^{+26.0}_{-7.3}$ eV with EW $= -5.7^{+4.6}_{-9.2}$ eV (errors denote 90 per cent confidence level).

Table 9. *Chandra* HRC-S/LETG observations of RX J0720.4−3125 in chronological order. We list the exposure times and the net counts after the data passed the GTI filters.

Obs. Id.	Start date	Counts 0.15–1.0 keV	Eff. exposure (ks)
368	2000 Feb 1	580	2.10
745	2000 Feb 2	3	0.14
369	2000 Feb 4	2660	6.12
5305	2004 Feb 27	9691	35.68
5581	2005 Jan 23	17 703	62.05
5582	2005 Jun 1	19 639	69.69
6364	2005 Aug 27	9323	31.68
6369	2005 Oct 8	4448	16.14
7177	2005 Oct 9	2067	7.18
7243	2005 Dec 14	4992	17.05
7244	2005 Dec 15	4295	16.16
7245	2005 Dec 16	2964	11.10
5584	2005 Dec 17	2972	10.87
7251	2006 Sep 9	2713	10.59
10861	2009 Jan 20	2948	11.11
10700	2009 Feb 14	5478	21.61
10701	2009 Sep 11	8228	32.36
11820	2010 Jun 19	8650	33.56
13181	2010 Nov 18	4937	19.90
13188	2010 Nov 19	3709	14.04
Total		118 000	429.60

and background) from both first orders were cut out within the standard LETG spectral extraction windows. The HRC-S/LETG spectra were added using the CIAO command 'ADD GRATING ORDERS' to add the two first orders (all other orders have a negligible count number) and 'ADD GRATING SPECTRA' to add the HRC-S/LETG spectra. To prepare the HRC-S/LETG data for spectroscopic fitting in XSPEC, the background was generated with the command TG−BKG. Altogether, the co-added HRC-S/LETG spectra have 429-ks exposure time (see Table 9). For details of the reduction of the *Chandra* data, we also refer to Hohle et al. (2010).

We fitted the co-added *Chandra* HRC-S/LETG spectrum of RX J0720.4−3125 with the same model as in Table 8 (without the narrow absorption feature at 0.57 keV), using the photons from 0.15–1.0 keV, but ignoring the edges of the chip gaps at 0.2390–0.2432, 0.248–0.252 and 0.2180–0.2215 keV, to avoid systematic fit errors. The fit yields χ^2/d.o.f. $= 1.07$ for 258 d.o.f., applying the standard model with blackbody radiation and the broad absorption feature at 0.3 keV. The spectral properties are listed in Table 10 and are consistent with those derived from *XMM–Newton* EPIC-pn spectra; see Hohle et al. (2009)[6] and Table 8. Note, the averaged temperature of RX J0720.4−3125 derived from the *Chandra* HRC-S/LETG spectrum (Table 10) is different to that obtained with the RGS data (Table 8), since the source is variable and the observations of the different instruments were performed at different times. In addition, possible systematic errors in the effective area calibrations between both instruments can lead to different temperatures.

The narrow absorption feature at 0.57 keV found by Hambaryan et al. (2009) should also be present in the co-added *Chandra* HRC-S/LETG spectrum of RX J0720.4−3125. Indeed, regarding the fit residuals in Fig. 8, such an absorption feature appears at the

Table 10. Fit results from the co-added *Chandra* HRC-S/LETG spectrum of RX J0720.4−3125 (blackbody with Gaussian absorption lines, where EW denotes the equivalent widths) and RX J1856.4−3754 (blackbody). The sizes of the emitting areas (norm) are calculated from the normalizations of the X-ray blackbodies and correspond to a distance of 300 pc for RX J0720.4−3125 (Kaplan et al. 2007; Eisenbeiss 2011) and 130 pc for RX J1856.4−3754 (Walter et al. 2010). All errors denote 90 per cent confidence level.

Model component	Unit	RX J0720.4−3125	RX J1856.4−3754
$N_{\rm H}$	10^{20} cm^{-2}	$0.886^{+0.048}_{-0.047}$	$0.800^{+0.033}_{-0.032}$
bbodyrad			
kT	eV	$92.4^{+0.9}_{-1.0}$	63.28 ± 0.48
norm	km	$4.5^{+1.3}_{-1.1}$	4.95 ± 0.12
Gaussian$_1$			
lineE$_1$	eV	$293.4^{+5.0}_{-6.9}$	–
σ_1 width	eV	$50.45^{+9.0}_{-7.1}$	–
EW$_1$	eV	$-29.6^{+4.7}_{-4.6}$	–
$\chi^2_{\rm red}$/d.o.f.		1.07/258	1.02/505
Gaussian$_2$			
lineE$_2$	eV	$482.6^{+5.1}_{-40.5}$	–
σ_2 width	eV	$7.8^{+9.0}_{-4.9}$	–
EW$_2$	eV	$-1.83^{+0.98}_{-2.76}$	–
Significance	σ	3.0	–
Gaussian$_3$			
lineE$_3$	eV	$529.4^{+2.2}_{-2.7}$	–
σ_3 width	eV	$3.8^{+2.9}_{-1.6}$	–
EW$_3$	eV	$-1.79^{+0.74}_{-0.84}$	–
Significance	σ	3.9	–
Gaussian$_4$			
lineE$_4$	eV	$566.4^{+6.6}_{-7.2}$	–
σ_4 width	eV	$7.4^{+5.3}_{-4.0}$	–
EW$_4$	eV	$-2.0^{+1.2}_{-1.3}$	–
Significance	σ	2.7	–
$\chi^2_{\rm red}$/d.o.f.		1.02/249	

[6] The EPIC-pn spectra are fitted for the individual observations in one session. Since RX J0720.4−3125 is variable, only $N_{\rm H}$, line energy and line σ are kept constant in time.

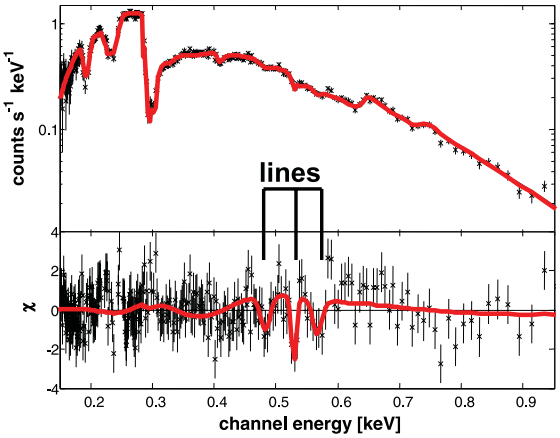

Figure 8. The co-added *Chandra* HRC-S/LETG spectrum of RX J0720.4−3125 with a total exposure of 429 ks. The black line represents the fit model, while the red line shows the fit model plus three narrow absorption feature seen at 0.48 keV, 0.53 keV and 0.57 keV, see also Table 10.

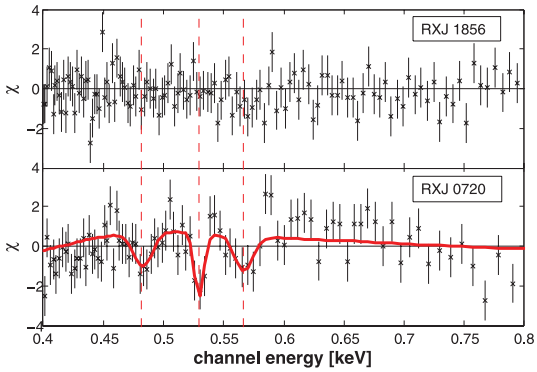

Figure 9. The fit residuals of RX J1856.4−3754 (see also Burwitz et al. 2001, 2003) and RX J0720.4−3125 obtained from the co-added *Chandra* HRC-S/LETG spectra. The absorption features (red solid line in the lower panel) seen in the residuals of RX J0720.4−3125 are absent in the residuals of RX J1856.4−3754. The red dashed lines mark the line centres of the three absorption features.

particular energy range, but less clear than in Fig. 1. Two other absorption features at 0.48 and 0.53 keV seem even more significant with respect to the continuum (Fig. 8), thus in addition to the narrow absorption feature found by Hambaryan et al. (2009), two other Gaussian absorption lines (at 0.48 and 0.53 keV) are added to the fit model.

Fitting the data with the additional lines, the fit yields χ^2/d.o.f. = 1.02 with 249 d.o.f. Since all lines are rather weak, for a cross-check *Chandra* pipeline products were used as well as reprocessed data for the co-added spectrum together with two different absorption models (phabs and tbabs) for the ISM and different grouping of the co-added spectra using the task GRPPHA. In all cases, the lines are present (see Fig. 8). The parameters of the absorption lines are listed in Table 10.

The absorption feature at 0.48 keV is not seen in the co-added RGS spectrum of RX J0720.4−3125, thus we also co-added all available *Chandra* HRC-S/LETG spectra of the much brighter NS RX J1856.4−3754 [for the individual observations, we refer to Burwitz et al. (2001, 2003); Drake et al. (2002)] for comparison.

For the fitting procedure we applied the same model as in Section 2.4. The fit results are listed in Table 10 and are in good agreement with the values published in Burwitz et al. (2001, 2003). The fit residuals of the *Chandra* HRC-S/LETG spectrum of RX J1856.4−3754 do not exhibit the absorption features we found in the fit residuals of the *Chandra* HRC-S/LETG spectrum of RX J0720.4−3125 (see Fig. 9). Thus, although weak, the features found in the spectrum of RX J0720.4−3125 are not of an instrumental origin.

4 DISCUSSION

The identification of narrow absorption lines in the X-ray spectra of highly magnetized NSs is non-trivial: if a line originates from the NS atmosphere, it is redshifted by a factor of $g_r = 1.11$ ($M = 1\,M_\odot$, $R = 16$ km) to $g_r = 2.00$ ($M = 2\,M_\odot$, $R = 8$ km) and the ion itself is not known. Considering abundances, lines in NS spectra may originate from highly ionized mid-Z elements or iron (Mori & Ho 2007), probably from the Kα lines, since they would cause the most strongest features. The strong magnetic field would shift and broaden the spectral lines.

An alternative interpretation is the interstellar origin of these absorption features, caused by the ISM, in particular in the LB; see e.g. Lallement et al. (2003) or Breitschwerdt & de Avillez (2006); Breitschwerdt et al. (2009). Some of the NSs in this work are likely located within the LB (e.g. RX J1856.4−3754), whereas other sources are outside (e.g. PSR B1055−52). We will discuss the two interpretations in the following sections.

4.1 Absorption features from the neutron star atmosphere

The detected line at 0.57 keV corresponds to O VII or O VI (Hirata & Horaguchi 1995) without gravitational redshift, as discussed in Hambaryan et al. (2009). This line is actually a blend that mainly consists of the Kα resonance line [$1s^2$–$1s2p^1P_1$(r)] at 573.95 eV of the triplet of He-like oxygen (O VII). This resonance line is superimposed with numerous weak O VI lines (see Hirata & Horaguchi 1995; Kaastra et al. 2009, for details), therefore the absorption feature at 0.57 keV appears not as a perfect Gaussian and the EWs and the linewidths (σ) are larger than expected from the single, fully resolved lines (note the resolution of RGS1 at 0.57 keV is ≈1.7 eV). The intercombination line [$1s^2$–$1s2p^3P_{1,2}$(i)] at 568.63 eV and the forbidden line [$1s^2$–$1s2s^3S_1$(f)] at 560.99 eV of the O VII triplet do not contribute to the absorption feature, since they appear only in emission (not detected in our spectra).

If highly ionized oxygen is present close to the NS surface, the O VIII Lyα line (1s–2p; i.e. O VIII Kα) at 653.62 eV could appear at ≈0.57 keV with a reasonable redshift of $g_r = 1.16$ (or $g_r = 1.17$) and the corresponding O VII Kα resonance line should appear at 0.48 keV ($g_r = 1.17$). In Hambaryan et al. (2009), it is argued that such an absorption feature may be detected in the co-added RGS spectra of RX J0720.4−3125.

We find no evidences for such a feature, neither in the co-added RGS spectra of RX J0720.4−3125 nor in the co-added RGS spectra of RX J1605.3+3249 (see Figs 1 or 3). The RGS detector exhibits an intrinsic feature at 0.48 keV that may superimpose a weak feature and inhibit a possible detection. However, we find such an absorption feature in the co-added *Chandra* HRC-S/LETG spectra of RX J0720.4−3125 (Figs 8 and 9). This feature is rather weak, but comparable (regarding to its broadness) to the absorption feature at 0.57 keV (Fig. 1), thus should be seen in the co-added RGS

spectra of RX J0720.4−3125 too (although superimposed by a much narrower instrumental feature).

Intriguingly, the absorption feature at 0.48 keV (if real, see Fig. 9) would fit the interpretation of a gravitational redshifted line (implying a redshift of $g_r = 1.17$)[7] and such features are expected at the particular energy range from NS atmosphere models (see Mori & Ho 2007, in particular fig. 14 therein for 10^{13} G field strength and 1 MK surface temperature, as measured for RX J0720.4−3125). On the other hand, the absorption feature at 0.48 keV is not very significant and requires further confirmation. The measured magnetic field strengths of the M7 (and the 3M) significantly increase the binding energy of atoms, if close to the NS. Under these conditions, the temperatures of ≈1 MK might be too low to generate significant amounts of highly ionized oxygen, as discussed in Hambaryan et al. (2009). However, the atomic physics is not well understood for magnetic fields of about $B \approx 10^{13}$ G.

Note, there is no such feature (at 0.48 keV) expected from the ISM [C VI would appear in this energy range, but significantly weaker (Hirata & Horaguchi 1995; Kaastra et al. 2009)]. An absorption feature at 0.65 keV (O VIII at rest, see Hambaryan et al. 2009) remains undetected, probably due to the lack of photons in this energy range (if from the ISM, the high temperatures that are required to generate O VIII are not likely).

The absorption feature found at 0.53 keV in the *Chandra* HRC-S/LETG data of RX J0720.4−3125 (see Fig. 8) likely originates from the K-edge of neutral oxygen O I (Kaastra et al. 2009) at rest. This indicates an overabundance of neutral oxygen in the line of sight or might result from inexact modelling of this edge. Although we use different ISM absorption models (e.g. phabs or tbabs), this particular feature remains.

The absorption feature at 0.57 keV is well detected in the *XMM–Newton* RGS spectrum of RX J0720.4−3125 (Hambaryan et al. 2009) and it appears (although weak) in the *Chandra* HRC-S/LETG spectra, i.e. its presence is certain (5.5σ significance in the RGS spectra). Moreover, a similar feature is also detected in the co-added RGS spectra of RX J1605.3+3249 [see van Kerkwijk et al. (2004) and Fig. 3]. The energies of the line centres are well fitted in both cases (Table 8), where the line centre of the absorption feature in the spectrum of RX J1605.3+3249 is shifted by ≈7.0 ± 4.5 eV with respect to the line centre of the absorption feature in the spectrum of RX J0720.4−3125. This shift cannot be explained by the same transition of a particular ion (e.g. O VII) at rest caused by different radial motion, since the required speed would be ≈3500 km s^{-1}. Either the two lines represent different transitions [$1s^2$–$1s2p^1P_1$(r) at 573.95 eV in the case of RX J1605.3+3249 and $1s^2$–$1s2p^3P_{1,2}$(i) at 568.63 eV in the case of RX J0720.4−3125; both for O VII at rest] – but that raises the questions why one transition is completely suppressed and why the intercombination line at $568.6^{+1.8}_{-1.9}$ eV (RX J0720.4−3125) is seen in absorption, not in emission. Alternatively, the shift might be caused by a slightly different gravitational redshift due to different NS compactness ($g_r = 1.14$ for RX J1605.3+3249) and both absorption features are caused by the O VIII Lyα/Kα line.

We found a similar feature at 0.57 keV in the co-added RGS spectrum of PSR B1055−52. However, the spectrum has not enough counts to identify this line undoubtedly and to determine the line energy of the line centre sufficiently accurate.

Note that spectral lines originating from the NS surface should appear split (and shifted) due to the Zeeman effect (Sarazin & Bahcall 1977) and broadened by pressure (Paerels 1997) that is not considered in this interpretation. Furthermore, the magnetic field is not constant over the NS surface, i.e. the lines should be broadened due to the contributions from different surface patches.

4.2 Absorption features of an interstellar or circumstellar origin

The distances of RX J0720.4−3125 and RX J1605.3+3249 are ≈195–530 pc (from direct parallax measurements; Kaplan et al. 2007; Eisenbeiss 2011) and ≈325–390 pc (estimated from extinction models; Posselt et al. 2007), respectively. Given the average volume density of O VII $n_{\rm O\,VII} = (1.35–2.84) \times 10^{-6}$ cm^{-3} in the ISM (assuming that oxygen is completely ionized to O VII; Yao & Wang 2005), the expected O VII column densities for these two NSs are $N_{\rm O\,VII} = (1.2 \times 10^{14})$–$(4.1 \times 10^{15})$ cm^{-2} and a factor of 2 or 3 larger for PSR B1055−52, since this NS is more distant (Kramer et al. 2003). The hydrogen column densities from these three NSs are in the order of $N_{\rm H} = 10^{20}$ cm^{-2} (Table 8). Applying the oxygen abundance relative to hydrogen ($n_{\rm O}/n_{\rm H} = 4 \times 10^{-4}$; Anders & Grevesse 1989), the expected column density of O VII should be in the order of $N_{\rm O\,VII} = 10^{16}$ cm^{-2} (again assuming that oxygen is completely ionized to O VII).

The measured EWs of the narrow absorption features at 0.57 keV yield $N_{\rm O\,VII} = 3 \times 10^{16}$–$10^{19}$ cm^{-2} (RX J0720.4−3125), $N_{\rm O\,VII} = 3 \times 10^{16}$–$10^{20}$ cm^{-2} (RX J1605.3+3249) and $N_{\rm O\,VII} \geq 10^{16}$ cm^{-2} (PSR B1055−52), taking fit errors (Table 8) and different velocity dispersions (Futamoto et al. 2004) into account and assuming that the absorption feature at 0.57 keV is a pure line (not a blend).

Hambaryan et al. (2009) discussed a possible circumstellar origin of the absorption feature at 0.57 keV in the RGS spectra of RX J0720.4−3125 to explain this difference of the column densities and showed that the absorption feature might be (partly) caused by an ambient medium surrounding RX J0720.4−3125 in ≈10^5 km distance from the NS, superimposed by absorption lines from the ISM. The model in Hambaryan et al. (2009) is also applicable to RX J1605.3+3249 and PSR B1055−52, since both NSs have temperatures and magnetic field strengths comparable to that of RX J0720.4−3125. However, circumstellar discs surrounding isolated NSs with ages of the order of million years should be rare. Thus, it is unlikely that three sources out of seven in our sample host a disc.

Regarding the EWs and the significance of the detection, the strongest narrow absorption features are present in the spectra of RX J0720.4−3125 and RX J1605.3+3249. Both NSs are located outside the LB (Lallement et al. 2003), i.e. they are embedded in a denser medium than in the solar vicinity. The LB hosts hot plasma containing highly ionized oxygen (Breitschwerdt & de Avillez 2006; Breitschwerdt et al. 2009), such as O VII or O VI that is in the line of sight to these NSs. In contrast, the closest NS, RX J1856.4−3754, is almost certainly located within the LB (the most recent parallax measurement yields a distance of ≈125 pc; see Walter et al. 2010) towards the Galactic Centre, i.e. embedded in a thin medium and therefore should not exhibit the narrow absorption feature.

The distance of RX J1308.6+2127 (RBS1223) is highly uncertain and ranges from ≈76 to 700 pc (see Haberl 2007, and references therein), but this NS has a high Galactic latitude and is located

[7] With this value, RX J0720.4−3125 would exceed its Schwarzschild radius by a factor of 3.7, i.e. would have an intrinsic radius of 15.6 km (assuming a mass of 1.4 $M_\odot$) or 18.3 km at infinity. However, the absorption features may originate from regions above the NS surface. Then, the given values for the radius are upper limits.

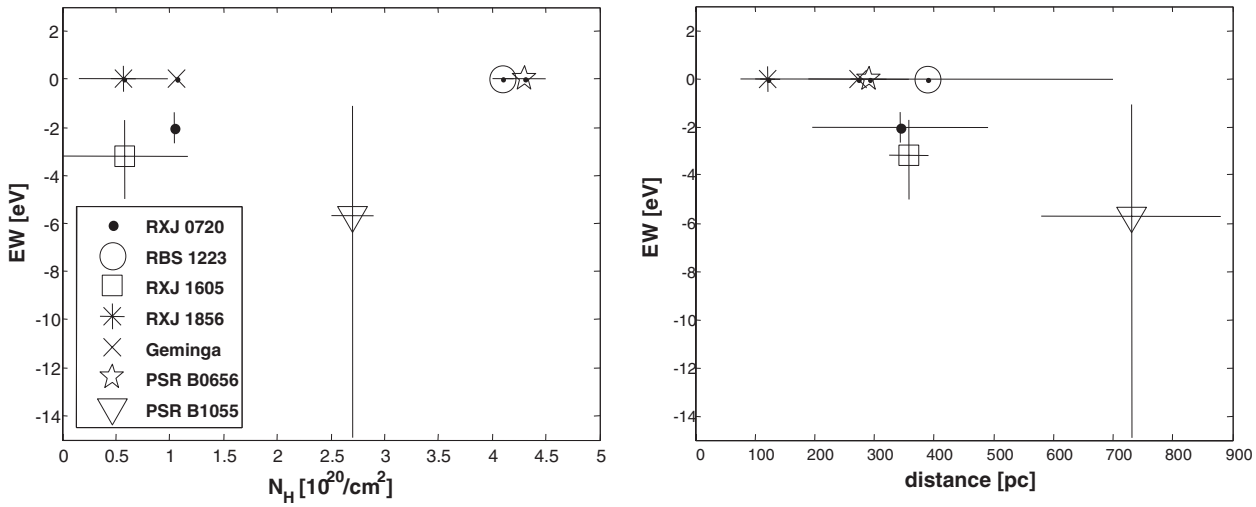

Figure 10. EWs of the narrow absorption features at 0.57 keV (errors denote 90 per cent confidence) as measured in this work compared to $N_{\rm H}$ and the distances of the '7' and the '3M'. The values and errors for $N_{\rm H}$ are obtained from EPIC-pn spectra (Haberl et al. 2003; van Kerkwijk et al. 2004; Hohle et al. 2009), in the case of the '3M' also from both EPIC-MOS (metal oxide semiconductor) (De Luca et al. 2005) and in the case of RX J1856.4−3754 from EPIC-pn and *Chandra* HRC-S/LETG spectra (Burwitz et al. 2001, 2003), note the different values for $N_{\rm H}$ obtained for EPIC-pn and LETG as published therein), since these spectra cover more of the soft part of the emission of the NSs than RGS, thus yield more reliable values for $N_{\rm H}$. The individual distances are obtained from the literature cited in the Sections 1.1, 1.2 and 2.

either within the LB (for smaller distances) or above the Galactic plane. Even in the latter case, RX J1308.6+2127 is still surrounded by a low-density medium [the local chimney; see Lallement et al. (2003), who shows the distribution of measured column densities]. Therefore, also the spectra of RX J1308.6+2127 should not exhibit narrow absorption features.

Geminga and PSR B0656+14 are located at roughly the same region above the Galactic plane, probably within the local chimney (the distances range from 150 to 300 pc for both objects; see Caraveo et al. 1996; Brisken et al. 2003; Walter 2005), like in the case of RX J1308.6+2127. Both NSs do not exhibit narrow absorption features, although in the case of Geminga the count number of the co-added RGS spectrum is too low to allow a final statement.

Finally, the spectrum of PSR B1055−52 shows an uncertain absorption feature and this NS is likely located outside the LB and is probably the most distant object in our sample [Kramer et al. (2003) estimated 750 pc from dispersion measurements].

If caused by the ISM, other X-ray sources (particularly much more distant) like e.g. Cyg X−2 (Yao et al. 2009), LMXB GS 1826−238 (Pinto et al. 2010, and other Galactic low-mass X-ray binaries; Yao & Wang 2005) or Mrk 421 (Kaastra et al. 2006; Rasmussen et al. 2007, with 955 ks exposure time) should exhibit similar absorption features. While the expected O VII resonance line at 573.95 eV of an interstellar origin is clearly visible (in particular in Kaastra et al. 2006, fig. 2 therein, and Rasmussen et al. 2007, fig. 1 therein), these sources do not show an absorption feature at 568.6 eV in their RGS spectra as detected in the case of RX J0720.4−3125. The line energy in the *Chandra* HRC-S/LETG spectra of RX J0720.4−3125 yields $566.4^{+6.6}_{-7.2}$ eV (Table 10), i.e. this value is almost compatible (within its errors) with the energy of the O VII Kα resonance line at rest.

5 CONCLUSIONS

We investigated the co-added RGS spectra of the four brightest M7 (RX J0720.4−3125, RX J1308.6+2127/RBS1223, RX J1605.3+3249 and RX J1856.4−3754) and the 3M (Geminga, PSR B0656+14 and PSR B1055−52), and searched for narrow absorption features, in particular at 0.57 keV.

We find that those NSs that are either nearby or located in a medium with low densities do not exhibit narrow absorption features, whereas those NSs that are distant and surrounded by a dense medium do exhibit narrow absorption features. The EWs of the narrow absorption features at 0.57 keV do not correlate with the $N_{\rm H}$ value, and hardly correlate with the distances (Fig. 10).

Other well-investigated X-ray sources (Cyg X−2, Yao et al. 2009; LMXB GS 1826−238, Pinto et al. 2010; Mrk 421, Kaastra et al. 2006; Rasmussen et al. 2007) do not exhibit an absorption feature at 568.6 eV as detected in the case of e.g. RX J0720.4−3125 (RGS). If this feature would have an origin in the NS atmosphere, the gravitational redshift and, thus, the compactness point either to a large radius and/or a small mass. However, we stress that the underlying atomic physics is not yet well understood for high magnetic field strengths.

ACKNOWLEDGMENTS

The *XMM–Newton* project is supported by the Bundesministerium für Wirtschaft und Technologie/Deutsches Zentrum für Luft- und Raumfahrt (BMWI/DLR, FKZ 50 OX 0001) and the Max-Planck Society. MMH acknowledges support by the Deutsche Forschungsgemeinschaft (DFG) through SFB/TR 7 'Gravitationswellenastronomie'. We thank Valeri Hambaryan for fruitful discussions, who encouraged us for this work, and the anonymous referee for helpful comments.

REFERENCES

Anders E., Grevesse N., 1989, Geochim. Cosmochim. Acta, 53, 197
Becker W., Truemper J., 1997, A&A, 326, 682
Bertsch D. L. et al., 1992, Nat, 357, 306
Bignami G. F., Caraveo P. A., Lamb R. C., 1983, ApJ, 272, L9
Breitschwerdt D., de Avillez M. A., 2006, A&A, 452, L1

Breitschwerdt D., de Avillez M. A., Fuchs B., Dettbarn C., 2009, Space Sci. Rev., 143, 263
Brisken W. F., Thorsett S. E., Golden A., Goss W. M., 2003, ApJ, 593, L89
Burwitz V., Zavlin V. E., Neuhäuser R., Predehl P., Trümper J., Brinkman A. C., 2001, A&A, 379, L35
Burwitz V., Haberl F., Neuhäuser R., Predehl P., Trümper J., Zavlin V. E., 2003, A&A, 399, 1109
Caraveo P. A., Bignami G. F., Mignani R., Taff L. G., 1996, ApJ, 461, L91
Caraveo P. A., De Luca A., Mereghetti S., Pellizzoni A., Bignami G. F., 2004, Sci, 305, 376
Cordova F. A., Middleditch J., Hjellming R. M., Mason K. O., 1989, ApJ, 345, 451
De Luca A., Caraveo P. A., Mereghetti S., Negroni M., Bignami G. F., 2005, ApJ, 623, 1051
de Vries C. P., den Herder J. W., Kaastra J. S., Paerels F. B., den Boggende A. J., Rasmussen A. P., 2003, A&A, 404, 959
de Vries C. P., Vink J., Méndez M., Verbunt F., 2004, A&A, 415, L31
den Herder J. W., Brinkman A. C., Kahn S. M. et al., 2001, A&A, 365, L7
Drake J. J. et al., 2002, ApJ, 572, 996
Eisenbeiss T., 2011, PhD thesis, Univ. Jena, Germany
Evans N. R., 1997, Chandra News, 5, 16
Fierro J. M. et al., 1993, ApJ, 413, L27
Futamoto K., Mitsuda K., Takei Y., Fujimoto R., Yamasaki N. Y., 2004, ApJ, 605, 793
Greiveldinger C. et al., 1996, ApJ, 465, L35
Haberl F., 2007, Ap&SS, 308, 181
Haberl F., Schwope A. D., Hambaryan V., Hasinger G., Motch C., 2003, A&A, 403, L19
Haberl F., Turolla R., de Vries C. P., Zane S., Vink J., Méndez M., Verbunt F., 2006, A&A, 451, L17
Halpern J. P., Ruderman M., 1993, ApJ, 415, 286
Halpern J. P., Wang F., 1997, ApJ, 477, 905
Hambaryan V., Neuhäuser R., Haberl F., Hohle M. M., Schwope A. D., 2009, A&A, 497, L9
Hirata R., Horaguchi T., 1995, Department of Astronomy, Faculty of Science, Kyoto University and National Science Museum
Hohle M. M., Haberl F., Vink J., Turolla R., Hambaryan V., Zane S., de Vries C. P., Méndez M., 2009, A&A, 498, 811
Hohle M. M., Haberl F., Vink J., Turolla R., Zane S., de Vries C. P., Méndez M., 2010, A&A, 521, A11
Jackson M. S., Halpern J. P., Gotthelf E. V., Mattox J. R., 2002, ApJ, 578, 935
Juda M., 1996, Chandra News, 4, 9
Juda J., 1997, Chandra News, 5, 20
Kaastra J. S., Werner N., Herder J. W. A. D., Paerels F. B. S., de Plaa J., Rasmussen A. P., de Vries C. P., 2006, ApJ, 652, 189
Kaastra J. S., de Vries C. P., Costantini E., den Herder J. W. A., 2009, A&A, 497, 291
Kaplan D. L., van Kerkwijk M. H., 2005, ApJ, 628, L45
Kaplan D. L., van Kerkwijk M. H., 2009, ApJ, 705, 798
Kaplan D. L., van Kerkwijk M. H., Anderson J., 2007, ApJ, 660, 1428
Kondratiev V. I., McLaughlin M. A., Lorimer D. R., Burgay M., Possenti A., Turolla R., Popov S. B., Zane S., 2009, ApJ, 702, 692
Kraft R. P. et al., 1997, in Siegmund O. H., Gummin M. A., eds, SPIE Conf. Ser. Vol. 3114, Performance and Calibration of the AXAF High-Resolution Camera II: the Spectroscopic Detector. p. 53
Kramer M. et al., 2003, MNRAS, 342, 1299
Kuntz K. D., 2009, in Smith R. K., Snowden S. L., Kuntz K. D., eds, AIP Conf. Ser. Vol. 1156, X-ray Evidence for the Local Hot Bubble. Am. Inst. Phys., New York, p. 3
Lallement R., Welsh B. Y., Vergely J. L., Crifo F., Sfeir D., 2003, A&A, 411, 447
Manchester R. N., Hobbs G. B., Teoh A., Hobbs M., 2005, VizieR Online Data Catalog, 7245, 0
Marshall H. L., Schulz N. S., 2002, ApJ, 574, 377
Mori K., Ho W. C. G., 2007, MNRAS, 377, 905
Oegelman H., Finley J. P., 1993, ApJ, 413, L31
Paerels F., 1997, ApJ, 476, L47
Pavlov G. G., Zavlin V. E., Sanwal D., 2002, in Becker W., Lesch H., Trümper J., eds, MPE Report 278, Neutron Stars, Pulsars, and Supernova Remnants. MPI, Garching, p. 273
Pinto C., Kaastra J. S., Costantini E., Verbunt F., 2010, A&A, 521, A79
Posselt B., Popov S. B., Haberl F., Trümper J., Turolla R., Neuhäuser R., 2007, Ap&SS, 308, 171
Posselt B., Neuhäuser R., Haberl F., 2009, A&A, 496, 533
Possenti A., Mereghetti S., Colpi M., 1996, A&A, 313, 565
Rasmussen A. P., Kahn S. M., Paerels F., Herder J. W. D., Kaastra J., de Vries C., 2007, ApJ, 656, 129
Sarazin C. L., Bahcall J. N., 1977, ApJ, 216, L67
Schwope A. D., Hambaryan V., Haberl F., Motch C., 2007, Ap&SS, 308, 619
Shelton R. L., 2009, Space Sci. Rev., 143, 231
Stairs I. H., 2006, J. Phys. G Nuclear Phys., 32, 259
Tetzlaff N., Neuhäuser R., Hohle M. M., Maciejewski G., 2010, MNRAS, 402, 2369
van Kerkwijk M. H., Kaplan D. L., Durant M., Kulkarni S. R., Paerels F., 2004, ApJ, 608, 432
van Kerkwijk M. H., Kaplan D. L., Pavlov G. G., Mori K., 2007, ApJ, 659, L149
Walter F. M., 2005, in Neutron Stars at the Crossroads of Fundamental Physics. Available at: http://www.physics.ubc.ca/~heyl/ns2005
Walter F. M., Eisenbeiss T., Lattimer J. M., Kim B., Hambaryan V., Neuhaeuser R., 2010, ApJ, 724, 669W
Yao Y., Wang Q. D., 2005, ApJ, 624, 751
Yao Y., Schulz N. S., Gu M. F., Nowak M. A., Canizares C. R., 2009, ApJ, 696, 1418

This paper has been typeset from a TEX/LATEX file prepared by the author.